

# Chapter 5

## Nanophotonic Approach to Energy-Efficient Ultra-Fast All-Optical Gates

Grégory Moille, Sylvain Combrié and Alfredo De Rossi

**Abstract** All-optical processing is based on fast nonlinear effects, such that light can be used to control light. The development of a novel class of low-loss semiconductor optical resonators, capable of field confinement close to the diffraction limit, has decreased the power level required to trigger nonlinear effects by several orders of magnitude. We review a decade of research on all-optical gates aiming both at fast and energy-efficient operation, with the prospect of integration on a silicon photonics platform.

### 5.1 Introduction: A Case for All-Optical Signal Processing

Data signals are ubiquitous in the everyday life and the resulting ever increasing demand in bandwidth for communication and processing is raising concerns about the alarming share of electric power they consume. This situation is producing a paradigm change in information technologies where photonics is promised to play a crucial role. The application domain of photonic technologies, originally centred on long-distance communication, is now extending to short-range data links and optical interconnects<sup>1</sup> as well as wireless and other microwave-related technologies [12, 44], particularly radar systems [22].

In future optical interconnect and other photonic assisted data processing systems, a large number of signals will be transferred into the optical domain and routed to the appropriate destination. Here, the question of minimizing the number of signal

---

<sup>1</sup>This topic is broadly covered elsewhere in this book.

G. Moille · S. Combrié (✉) · A. De Rossi  
Thales Research and Technology, 1, av. A. Fresnel, Campus Polytechnique,  
91767 Palaiseau, France  
e-mail: sylvain.combrie@thalesgroup.com

A. De Rossi  
e-mail: alfredo.derossi@thalesgroup.com

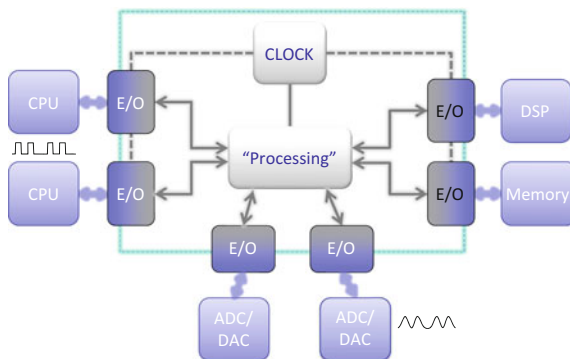


**Fig. 5.1** Possible synergy between electronics and fast optical processing where all-optical routing is used to avoid additional conversion in the electric domain

conversions from and to the electric domain becomes relevant. As an example, performing any sort of “operation”, for instance detecting the header of a message or extracting a subset of data from a high speed channel, requires the conversion into the electric domain. Thus, these signals need to be detected, processed, and reconverted into the optical domain. Thus, wherever possible, it would be convenient to have some of these operations to be performed in the optical domain. This situation is represented in Fig. 5.1, where digital and analog data are converted in the optical domain for transmission and for a few critical operations such as pattern search. Optical signals are also needed for synchronisation and precise analog to digital conversion [22, 76].

Optical correlation techniques are in principle extremely effective for pattern search, and could be used to reduce the amount of data to be processed by electronics drastically [81]. This is shown in Fig. 5.2. Another example of all-optical processing being implemented with fibre optics and bistable optical elements is the all-optical header recognition and signal routing [19].

In this book chapter, a critical optical function named all-optical gating (AOG) is considered. This consists in sampling an optical signal at an extremely well defined time, which is controlled by another optical signal. A related application domain of all-optical gates is Optical Time Domain Division (OTDM). OTDM is a convenient alternative to more complex signal modulation formats when high-speed and simplicity, but not spectral efficiency, matters, e.g. in dedicated communication links, optical interconnects or other kinds of short-range but high-speed channels. Also, high-speed signal measurement techniques are based on optical gating [79].

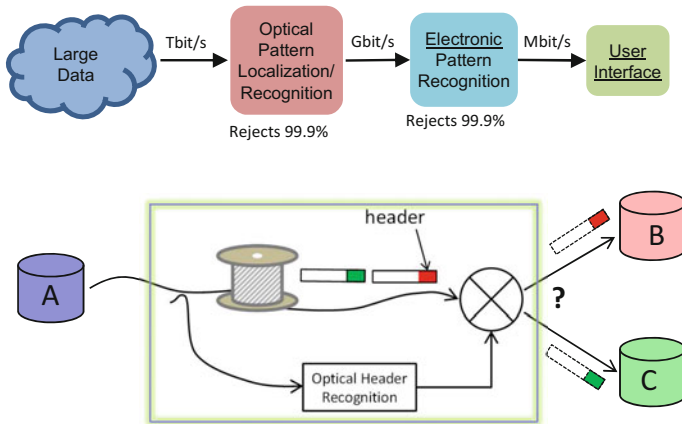


**Fig. 5.2** All-optical processing could be effective for fast information retrieval, as a front-end to electronics. Top, optical techniques could be used to search for a specific information within a large amount of data; bottom, scheme for all-optical routing. Adapted from [81]

## 5.2 Integrated All-Optical Gate

### 5.2.1 Technologies for Integrated On-Chip All-Optical Processing

All-optical gates are based on fast nonlinear effects. One of the most popular implementation of this concept is the nonlinear optical loop mirror (NOLM), widely used for ultra-fast all-optical manipulation of high-speed optical signals [51]. It exploits the nonlinear index change (Kerr effect) in a Sagnac fibre interferometer [18]. The NOLM is an extremely fast (sub-ps gating time), simple and robust device where the intrinsically weak nonlinear response of silica is compensated by the large interaction length (> 100 m) and very low losses, which makes operation with Watt-level peak power pump possible.

The seek for an integrated equivalent of the nonlinear optical fibre started in the late 80's and considered semiconductors [68] because of their nonlinear response, about 3 orders of magnitude larger than in Silica [62]. Semiconductor integrated optics has taken off almost two decades later, however, with the fabrication of low-loss and tightly confined waveguides [21, 65].

In parallel, the large and relatively fast optical nonlinearities in active semiconductor devices, in particular semiconductor optical amplifiers SOA, have raised considerable interest [26, 43] for high-speed all-optical signal processing. Recently, SOAs have been operated as fast optical gates with close to 100 Gb/s data rate, based on Cross-Phase-Modulation in a Quantum Dot active region [47]. Even faster operation have been achieved in similar devices by exploiting Four-Wave-Mixing [46]. The underlying dynamics of free carriers here is characterized by a slow time constant

( $\approx 100$  ps) requiring special care (e.g. differential mode architectures with two SOAs) to avoid undesired patterning effects.

An original and conceptually elegant approach consists in inducing a change of absorption and refractive index via an intersubband transition. This prevents any slow dynamics related to the generation/recombination process to interfere with the evolution of the distribution of free carriers in the conduction band, which is a much faster process. The concept has been implemented using a double quantum well structure with transition energy in the Telecom spectral range owing to Antimonide alloy structure grown on Indium Phosphide [17]. Truly picosecond nonlinear switching with picojoule pump energies have been achieved and an integrated switch capable of demultiplexing a data stream at 160 Gb/s has been demonstrated [3]. A very strong nonlinear response of Silicon nanocrystals has been reported recently [45].

An overview of the possible all-optical gating technology is shown in Fig. 5.3, with particular emphasis on resonant devices, namely ring resonators or photonic crystals. For comparison, non-resonant devices such as nonlinear waveguides and interferometers are also represented.

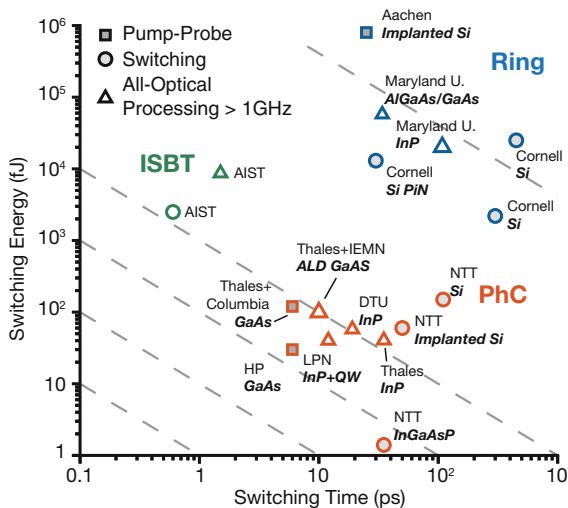


**Fig. 5.3** All-optical processing based on semiconductor nonlinear devices, compared in terms of the speed (the switching time or recovery time) and the energy required for triggering the switching action. Symbols refer to different situations: pump-probe measurement of the response, direct observation of switching (or gating) and operation at high rate. Dashed line represent a constant  $time \times energy$  product, which is approximately conserved for the same material and same cavity design

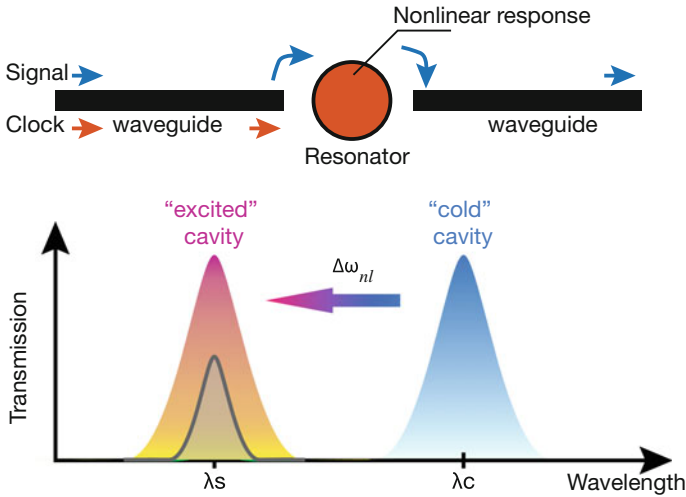


**Fig. 5.4** Principle of the resonant all-optical switch. Signal is modulated by the dynamical control of the detuning

### 5.2.2 Energy-Efficient All-Optical Gates

The first attempt to build what at that time was described as the optical equivalent of a transistor dates back to the 70's. It was shown that an optical resonator (a Fabry-Pérot interferometer) filled with a nonlinear material (Na vapour excited near the  $D$  absorption lines) responds with a characteristic bistable input-output dependence [24]. III-V semiconductors have quickly been considered as more suitable materials for miniaturization and for improving speed and energy efficiency [23]. That leads to the concept of nonlinear semiconductor resonator as all-optical gates meant to operate at reasonably low optical power levels.

Considerations about the benefits of scaling down the volume of the resonator have motivated research on monolithic semiconductor resonators made of GaAs [33], where it was shown that recovery time and the pulse energy required for optical control decrease with the size of the resonator. Fast recovery time (30 ps) and strong all-optical modulation have been achieved with a pump pulse energy of about 600 fJ, in the smallest device.

Optical integrated circuits built around nonlinear resonators have been proposed later [77] to perform some all-optical processing experiments, particularly wavelength conversion, whereas a modulated signal at wavelength  $\lambda_1$  is used to modulate a CW carrier at  $\lambda_2$ . As for semiconductor waveguides, the recent improvement of processing capabilities, enabling high-quality etching and, even more importantly, sub-micron patterning, has enabled a radically new class of optical microresonators, combining both small size and large quality factor.

In order to appreciate how this point is important in the context of all-optical gates, it is useful to consider two parameters characterizing their operation: the energy required for switching ( $E_{sw}$ ) and the recovery time ( $\tau_r$ ). In the specific case of nonlinear resonators, with quality factor  $Q$  and mode volume  $V$ , and in the continuous wave limit, it is shown that the minimum power for observing bistable switching is  $P_{min} \propto n_2 V Q^{-2}$  [67], when assuming instantaneous (e.g. Kerr) index change  $\Delta n = n_2 I$ . Based on scaling rules for  $n_2$  with the energy gap of the semiconductor, it has been shown that the nonlinear response within a given spectral range can be maximized with a suitable choice of the semiconductor compound alloy [63, 68].

Assuming the choice of the most suitable material has been made, which also depends on other parameters such as manufacturability, cost, and other optical properties, the same relation suggests a connection between the device bandwidth, namely the recovery time,  $\Delta\omega = 1/\tau_r \propto Q^{-1}$ , and the operating power  $P_{min} \approx E_{sw}/\tau_r$ , *i.e.*:

$$E_{sw}\tau_r = const \times n_2 V \quad (5.1)$$

Therefore, increasing the Q factor will reduce the switching energy, but at the cost of reducing the speed too. Instead, the reduction of the modal volume could, in principle, improve energy efficiency without affecting speed. There is an interesting similarity with microelectronics, where the decrease of energy consumption *per transistor* has decreased drastically by mere geometrical scaling considerations.

The modal volume express the capacity of a resonator to store light within a certain volume, and it is related to the spatial distribution of the field  $\vec{E}(\vec{r})$  of a particular normal mode. More precisely,  $V$  is the volume that an uniform field  $E = \max(\vec{E}(\vec{r}))$  would need to store the same amount of energy as in the resonator, namely:  $W = \frac{1}{2} \int \epsilon_0 \epsilon_r |\vec{E}(\vec{r})|^2 d\vec{r} = V \times \frac{1}{2} \int \epsilon_0 \epsilon_r \max(|\vec{E}|^2)$ , as illustrated in Fig. 5.5.

Extremely large Q-factors are possible in dielectric resonators [75], while, as the equations above suggests,  $V$  is only loosely related to their physical footprint. The important point here is that if the index contrast is large enough, the optical mode is in general well confined inside the resonator and can approach the diffraction limit  $(\frac{\lambda}{2n})^3$ .

Plasmon resonators can beat this limit [52], but at the cost of large optical losses, because in this limit the magnetic energy of the resonant mode is vanishing and is replaced by the kinetic energy of electrons in the metal, which is dissipated within the short timescale of inelastic collisions (10–100 fs) [36], setting a limit to the Q factor which is too severe for exploiting the resonant enhancement.

Dielectric resonators made of silicon (or other high index materials) such as micro-rings or micro disks (Fig. 5.5), can achieve a much larger Q factor ( $> 10^6$ ) while the smallest ring resonator [58] with radius = 1.5  $\mu\text{m}$  features a mode with volume  $V \approx 1 \mu\text{m}^3$  which is way smaller than macroscopic resonators or other dielectric resonators with low refractive index contrast, but still nearly 2 orders of magnitude larger than the diffraction limit, namely  $(\frac{\lambda}{2n})^2 = 0.015 \mu\text{mm}^3$  in the telecom C band. The measured intrinsic Q factor is  $2 \times 10^4$ , about a factor two below the bending loss limit for this radius.

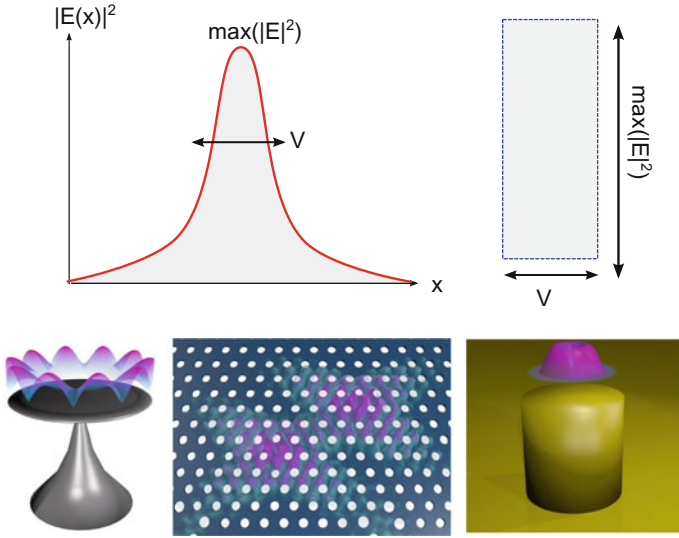


**Fig. 5.5** Optical resonators. *Top* Concept of the modal volume:  $V$  is such that it contains the same energy as the resonator when filled with uniform field  $E = \max E(\mathbf{x})$ . *Bottom* representation of some categories of resonators, micro-disk, PhC and plasmonic resonator

Instead, Photonic Crystal (PhC) resonator can approach this limit much closer. The design developed by Zhang and Qiu [88] results into a mode volume of  $0.03 \mu\text{m}^3$ , only twice as large the diffraction limit. Thus, semiconductor PhC resonators are extremely suited for maximizing speed and energy efficiency.

### 5.2.3 III–V Photonic Crystals Resonators

Photonic Crystals are optical structures whose properties are modulated periodically at the scale of the wavelength. They can be viewed as a generalisation of the Bragg reflector, where the scattered waves add coherently to produce a reflection with strength growing with the number of periods of the reflector. Consequently, a perfectly ordered and infinite structure, periodically modulated along any direction, forbids the propagation of light within a given spectral range. The existence of a forbidden gap for photons implies fundamental properties in the control of the light-matter interaction [82]. In analogy to semiconductors and crystals, a “defect” in an otherwise perfectly periodic structure results into resonant localized states [34].

The fabrication of such structures has been attempted with *ad hoc* techniques (e.g. holography) but is still extremely challenging because of the tight tolerances required. In contrast, the planar semiconductor patterning and etching processes, derived from microelectronics, can meet such tolerances. Crucial milestones have

been the demonstration of a complete photonic band gap along the plane of such structures [39] and the first laser [56]. These two-dimensional structures needed to be optically isolated from the substrate, in order to avoid off-plane radiation losses [35]. This was achieved through the removal by chemical etching of the “sacrificial” layer beneath the patterned area, which leaves a self-standing membrane, as shown in Fig. 5.6.

The careful design of the “defect” is crucial in order to induce a strong optical confinement and a large Q-factor [2]. The continuous improvement of the design and of the processing has led to the achievement of very large Q (up to  $10^7$ ) factors [61].

A different optimisation leads to the minimisation of the mode volume, which is more relevant for fast optical gates. A very suitable design [88] consists in displacing two holes by a fraction (0.16) of the lattice period, which is shown in Fig. 5.6. This produces a resonance close to the high frequency side of the forbidden photonic gap of the lattice (and it is therefore referred as a “donor” mode). The corresponding distribution of the optical field is extremely localized, mostly between the two displaced holes. The calculated mode volume is  $0.24(\lambda/n)^3$ , which is less than twice the diffraction limit.

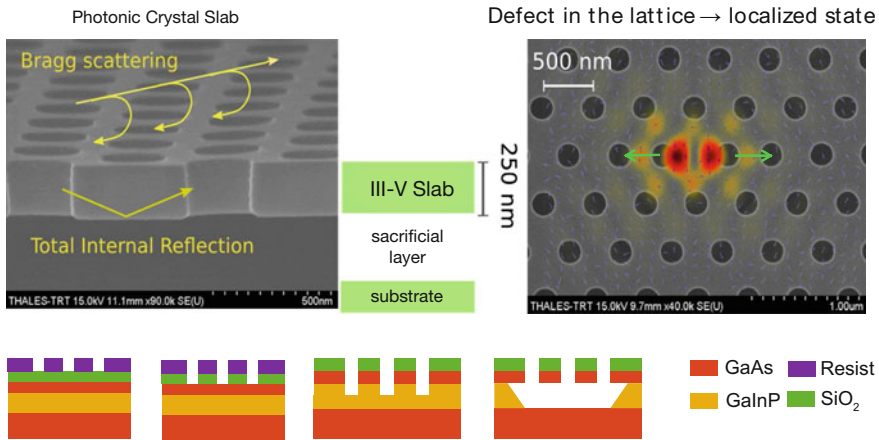


**Fig. 5.6** Photonic crystal made of a semiconductor membrane patterned with a two-dimensional lattice of holes. *Left* in-plane confinement results from the Bragg scattering (the photonic band gap), out-of-plane confinement is ensured by total internal reflection. *Right* defect-mode resonator resulting from the outward displacement of two holes; intensity of the electric field is superimposed. The cavity design is based on [88]. Process flow, from *left* to *right* resist patterning by e-beam lithography, etching of the  $\text{SiO}_2$  hard mask, etching of the III-V by an Inductively Coupled Plasma (ICP) and removal of the sacrificial layer. The fabrication process is detailed in [14]



### 5.3 Nonlinear Dynamics in PhC Resonators

Long ago, S. John suggested *the utilisation of localisation as a trigger mechanism for nonlinear or bistable response, as in the Kerr electro-optic effect* in photonic crystals [34]. The nonlinear dynamics of PhCs has indeed been investigated broadly [32, 66], highlighting phenomena such as non-adiabatic dynamics [83], wavelength conversion [54], self-pulsing [13, 41], to cite a few. The focus here will be on how such cavities can be designed to achieve energy-efficient and fast all-optical gating in a device which could be compatible with photonic integrated circuits. These considerations have strong implications in the choice of the materials and designs, which will be discussed hereafter.

#### 5.3.1 Microwatt Nonlinear Response

Photonic crystals cavities are almost single mode resonators with mode size comparable to the wavelength. The density of the optical power can be extremely high compared with the level of the power at the input. In the coupled mode approximation [42], the energy in the cavity  $W$  is simply related to the input power  $P$  through the cavity photon lifetime  $\tau_c = Q\omega_0^{-1}$ , namely  $W = P\tau_c$ . Let us consider a cavity with a mode volume  $V = 1.3(\lambda/n)^3$  and  $Q \approx 10^6$  fed with  $P = 1 \mu\text{W}$  and  $\lambda = 1.5 \mu\text{m}$ . While the stored energy at steady state is only 5 fJ, the energy density is as large as in a beam with  $I = 1 \text{ GW/cm}^2$ , which is enough to trigger the nonlinear absorption in semiconductors such as GaAs.

This situation is apparent in Fig. 5.7, where the resonance of a high-Q cavity ( $5 \times 10^5$ ) is broadened due to nonlinear absorption as the coupled input power is in the micro-Watt range [15]. The heat generated by the nonlinear absorption in the cavity can be estimated through its thermal resistance from the observation of the rise of the local temperature. In GaAs, the thermal resistance of these structures is typically about  $10^5 \text{ K/W}$ . This is a large value, as at steady state, or a times scales longer than the thermal time constant (in the  $\mu\text{s}$  range), a few microwatts of absorbed optical power induce an index change much larger than any other nonlinear effect (Kerr or due to free carriers). Thermal nonlinearity is therefore the dominant effect at long time scales. Bistable transitions are easily observed when the excitation is red detuned relative to the cavity resonance [80].

In the context of ultra-fast all-optical processing, however, the thermo-optic effect is too slow to be exploited, but still need to be considered carefully in order to achieve a stable operation point.

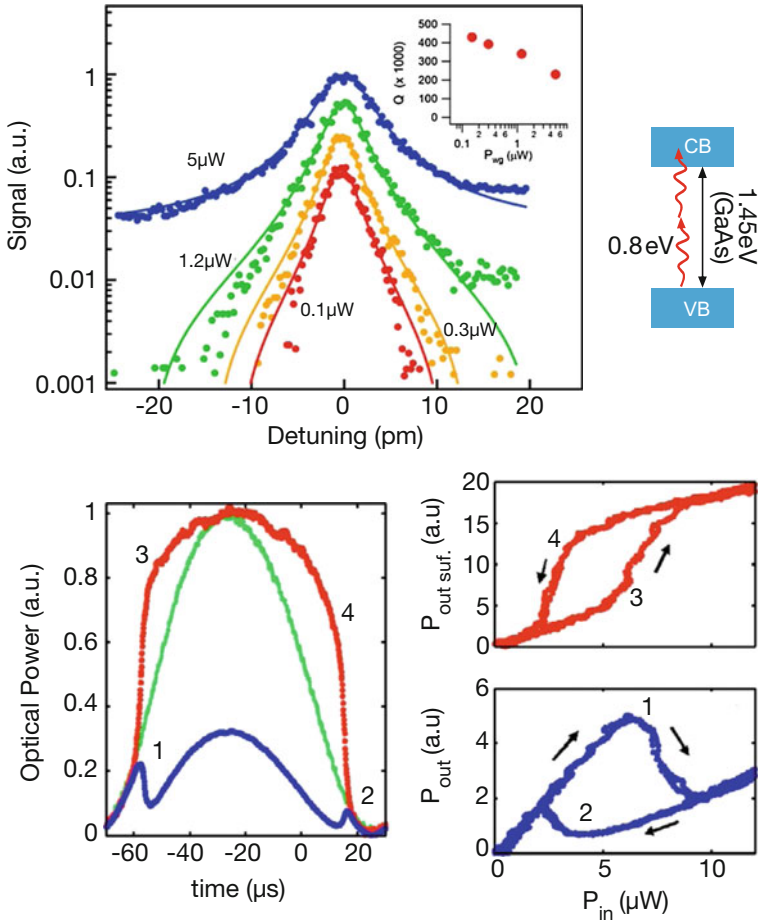


**Fig. 5.7** Broadening of the resonance of a high-Q GaAs PhC cavity due to nonlinear absorption, from [15]; bistable response of a GaAs cavity due to thermally induced index change, from [80]

### 5.3.2 Fast Optical Nonlinearities in Semiconductors

In semiconductors, the contribution to the nonlinear index change due to the anharmonicity of the electron potential, i.e. the Kerr effect, is in general weaker than that resulting from the excitation of free carriers. This latter contribution consists of a variety of different mechanisms. The first of these is captured by the Drude model, describing a plasma of charged particles interacting with an electromagnetic field. As the density of free carriers increases, this results into a decrease of the refractive index at optical frequencies above the plasma resonance, which, in this case, is located in the THz spectral range or below. The second mechanism, “band filling”, is related to the saturation of the absorption as states in the conduction band are filled

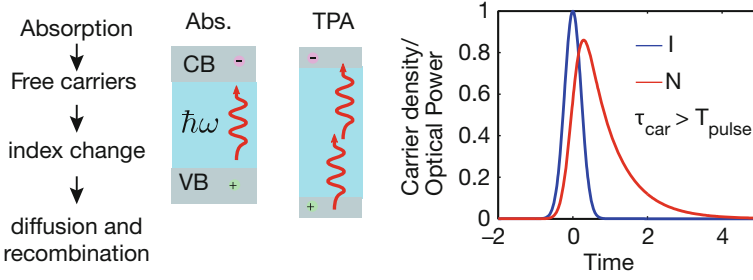


**Fig. 5.8** The nonlinear response (normalized units) to optical excitation  $I$  in semiconductors is dominated by the free-carriers dependent refractive index, which is not instantaneous, as it follows the carrier density  $N$

up. This also induces a decrease of the refractive index, described by the Kramers-Kronig equations. The third effect is explained as a many-body effect inducing a “shrinkage” of the electronic band gap, hence a change of the dispersion [9].

On the other hand, carrier dynamics is not instantaneous, as it is regulated by diffusion and recombination, with a rate  $\tau_{carr}$  typically in the picosecond to nanosecond time scale (Fig. 5.8). The simplest model is based on the rate equation  $\dot{N} = -N/\tau_{carr} + \frac{\alpha}{\hbar\omega}I$ , with  $\alpha$  the linear absorption. The change of refractive index  $\Delta n = \frac{dn}{dN}$  is dispersive, and it is particularly large near the absorption band edge of the semiconductor [9].

In the limit where recombination is much faster than the excitation,  $\tau_{carr} \ll T$ , an effective Kerr nonlinear response can be defined as  $n_2 = \frac{dn}{dN} \frac{\tau_{carr}}{\hbar\omega} \alpha$ . For *GaInAsP* with electronic gap  $E_g = 0.84$  eV (1470 nm) the absorption at  $\lambda = 1.55$   $\mu\text{m}$  is  $\alpha = 300 \text{ m}^{-1}$  and  $\frac{dn}{dN} = -8 \times 10^{-20} \text{ cm}^{-3}$ , thus  $n_2 = -3 \times 10^{-15} \text{ m}^2\text{W}^{-1}$ , assuming  $\tau_{carr} = 20$  ps. This value is more than 2 orders of magnitude larger than the electronic Kerr contribution. Based on a combination of optimized nonlinear response of the material and confinement in a ultra-small cavity, all-optical switching with femto-Joule control pulses has been demonstrated in PhC cavities [55].

Because of the large density of the optical field in the cavity, non-linear absorption is in general not negligible. In *GaInAsP* (0.84 eV), the nonlinear absorption is comparable to direct absorption as the power intensity is  $0.2 \text{ GW cm}^{-2}$ , which is easily reached in PhC cavities. Thus, semiconductor with relatively large gap, such as GaAs (1.42 eV), InP (1.35 eV) and Silicon, and, therefore, strictly transparent at the telecom wavelengths, can be used for nonlinear gates in this spectral range. The weaker index dependence on the carrier density implies however slightly larger power levels.

Nonetheless, there are two advantages in using binary material such as GaAs and InP: the much better thermal conductivity than ternaries, and the transparency of the material in the linear regime. Thus, the signal (probe) can be made weak enough not to induce nonlinear effects itself, and, furthermore, the same material can be used for in-plane propagation of signal and pump. Thus, it is not necessary to excite the cavity off-plane or to develop a complex 3D optical circuitry.

### 5.3.3 Nonlocal Nonlinear Response of PhC Cavities

The geometry of the optical resonators considered here has two important implications on the dynamics of free carriers, hence of the nonlinear response. First, the average distance of the photo-generated carriers from the surface  $L_s$  is very short (typically 100 to 200 nm) compared to the diffusion length. Thus, surface recombination  $S$  tends to dominate any other recombination process. In the case of *GaAs*,  $S$  might approach the saturation velocity in absence of any passivation treatment [53]. Considering a patterned surface such as in PhC crystal structures, an effective carrier lifetime is readily derived within the Shockley [64] approximation:  $\tau_{eff}^{-1} = \tau^{-1} + S/L_s$ , which can be shorter than 1 ps. Such a fast dynamics was first observed in *GaAs* Photonic Crystal structures [11].

The second implication of the nanoscale geometry appears when the photogeneration is localized within a range smaller than the diffusion length, or the distance to the surface. Then, a new time constant appears in the evolution of the carrier density, which is related to the migration of carriers away from the area where the optical cavity mode is localized. This becomes apparent when the recombination process is less important, such as in material with weaker surface recombination, such as *InP* or *Silicon*. In order to appreciate this point, Fig. 5.9 shows the decay of the carrier density in the area where the optical field is localized, which we refer to as *effective density*  $N_{eff}$ . The very early stage is characterized by a time constant which is almost two orders of magnitude faster than the effective carrier lifetime (about 500 ps in *InP* PhCs). The origin of this behaviour is apparent when observing the spatial distribution of photogenerated carriers, initially localized within about half a micron, and expanding very quickly in the first picoseconds. This effect was first observed in *silicon* PhCs [72] and later in other semiconductors, namely *InP* [29, 87] and *InGaAsP* [55].

When the surface recombination is large, then it can compete with diffusion. Figure 5.10 compares the decay of the effective density  $N_{eff}$  with the averaged density, i.e. the total carrier population, as the surface recombination is increased. While the total carrier population decays exponentially with a time constant clearly related to the recombination, the effective density is also influenced by the diffusion, which is increasingly apparent as  $S$  decreases.

It has been realised that, in nanoscale semiconductor resonators, the exponential decay described by a time constant is not well adapted to describe the nonlocal response of carriers. Very recently, a model based on the Green's function has been introduced to provide a more accurate description of the diffusion process [48].

## 5.4 PhC All-Optical Gate

The concept of a resonant all-optical gate, as illustrated in Fig. 5.4, has been first implemented in a photonic crystal structures on a *Silicon on Oxide* platform [71],

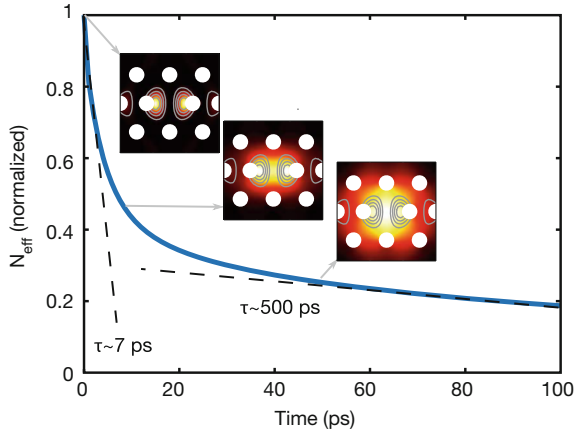


**Fig. 5.9** InP PhC cavity. Calculated effective density of carriers  $N_{eff}$ , generated by TPA in a PhC cavity. Snapshots of the spatial distribution are shown at the excitation, after fast diffusion ( $\approx 7$  ps) and after 50 ps. The lattice period 450 nm gives the spatial scale. Gray contour lines denote the initial carrier distribution, added for comparison. Dashed straight lines denote fitted fast and a slow time-constants

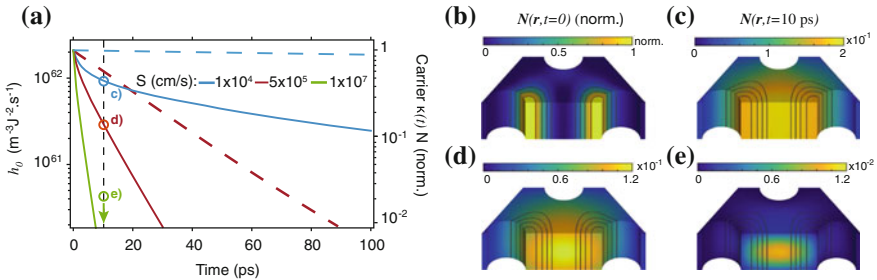


**Fig. 5.10**  $H_0$  cavity: calculated impulse response  $h_0$  (solid) and the spatially averaged and normalized carrier density  $\kappa(t) = \overline{N}/\max(\overline{N})$  (dashed), depending on the surface recombination velocity  $S$ . Initial ( $t = t_0$ ) spatial distribution  $N$  of the carriers (b) and at  $t = t_0 + 10$  ps with (c)  $S = 10^4$  cm s $^{-1}$ , d  $S = 5 \times 10^5$  cm s $^{-1}$  and e  $S = 1 \times 10^7$  cm s $^{-1}$ . Adapted from [48]

shortly following the demonstration of a nonlinear ring resonator on the same material [4]. Arguably, this opened the perspective of making these nonlinear devices accessible through mass-production, and attractive because they can coexist with the wide palette of photonic functions already available on this platform.

Still, the nonlinear absorption coefficient, the carrier mobility and lifetime in Silicon are not the most favourable for fast all-optical processing, compared to other materials, particularly III–V semiconductors. Faster and more energy-efficient devices are possible by selecting materials with faster carrier lifetime and stronger nonlinear response. The choice of the appropriate cavity design, minimizing the modal volume is also crucial, as discussed in Sect. 5.2.2.

Figure 5.11a represents a PhC all-optical gate obtained by evanescently coupling a  $H_0$  resonator to two PhC waveguides. The  $H_0$  cavity design, described in detail in Fig. 5.6, provides the smallest modal volume for a dielectric resonator. Moreover, the choice of *GaAs* allowed to exploit its large surface recombination and one order of magnitude larger nonlinear absorption compared to Silicon, translating into much faster and more energy-efficient operation [30].

The quality factor of the resonator is estimated from the transmission spectrum (Fig. 5.11b). The coupling loss into the waveguide, here  $\sim -5$  dB/facet, is reasonably small owing to a mode-adapter which is detailed in [74]. The linear transmission is estimated to be 90% with the cavity on-resonance, which corresponds to the ratio between the loaded  $Q_L = \lambda_0/\Delta\lambda = 1200$  and the intrinsic  $Q_i = 2.5 \times 10^4$ . The cavity photon lifetime  $\tau_{ph} = Q_L \lambda_0 / 2\pi c \approx 1$ ps is short enough not to limit the switching speed.

Homodyne wavelength-degenerate pump-probe measurements reveal all-optical modulation, with an increase or a decrease of the signal, depending on the detuning (Fig. 5.11c, d). In both cases, a decay constant close to 6 ps is observed, suggesting a much faster carrier dynamics than in other semiconductor, e.g. Silicon [71], no matters if it is implanted with ions to decrease the carriers lifetime [70]. Recent measurements on GaAs PhC cavities designed to operate in the near infrared spectral range have also concluded a fast carrier lifetime [10]. It is likely that  $\tau_{carr}$  might however vary substantially in GaAs nanoscale structures, likely in the 1 – 10 ps range, depending on the detail of the etching process used to pattern the PhC structure and,

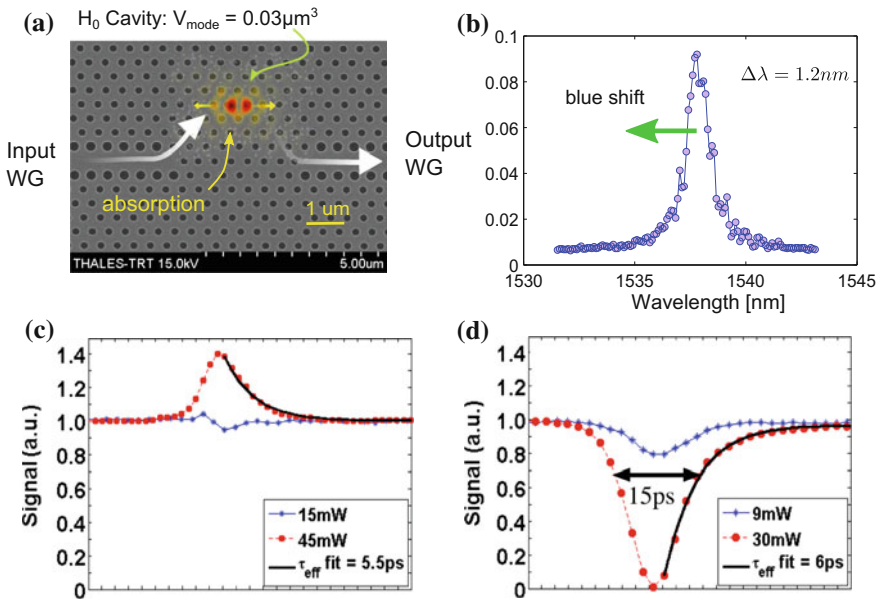


Fig. 5.11 GaAs-based PhC resonant all-optical device, following [30]

more generally, on the properties of the surface. This point will be discussed further in Sect. 5.4.5.

Another remarkable aspect of this GaAs structure is the low power level inducing the all-optical modulation, which is below 50 mW peak, hence about 200 fJ for a 4 ps long pulse. This is the result of the extremely tight optical confinement and the large nonlinear absorption. How this compares with other technologies and materials is represented in Fig. 5.3.

### 5.4.1 Photon Molecule

The practical use of nonlinear gates requires that the optical control can be distinguished from the signal. In principle, the symmetries of a doubly degenerate resonance could be exploited to avoid unwanted crosstalk. Nevertheless, the spectral separation of the signal and the control is much easier to implement, as this requires a doubly resonant cavity and filters. The so called  $L_3$  and  $L_5$  cavities (3 and 5 missing holes in line) contain several modes and have been used for frequency non-degenerate all-optical switching [71].

A crucial point here is that the strength of a non-degenerate nonlinear interaction depends on the spatial overlap of the electric fields. This is strictly true for the Kerr interaction (and Four Wave Mixing). It could be speculated that this conditions could be relaxed, since the free-carriers induced index change, which is exploited here as nonlinear effect, is non-local, as discussed in Sect. 5.3.3. In practice, and particularly if the effective carrier lifetime is short, achieving a good field overlap, e.g. spatial matching of the two resonances, remains critical for maximizing the nonlinear response.

The above constraints lead to the concept of “photon molecule”, where coupling two single-mode cavities results into a doublet of resonances [27, 31, 73], is used here to obtain two modes maximizing their overlap. The photon molecule is implemented here using two  $H_0$  cavities separated by 4 lattice periods along the  $M$  direction [16, 50], as shown in Fig. 5.12a. The symmetric and anti-symmetric combination of the  $H_0$  cavity mode are associated to the two resonances (Fig. 5.12b, c). The amplitude  $|E|$  of these two super-modes overlaps almost perfectly (Fig. 5.12d), which is what matters here. As a consequence, the excitation of either modes results into a close to identical spectral shift of both of them (Fig. 5.12b), thereby enabling efficient non-degenerate switching, i.e. with spectrally separated signal and control optical channels.

### 5.4.2 The Role of the Carrier Lifetime

In a semiconductor all-optical device based on the excitation of free-carriers, the density of the effective carrier population  $N_{eff}$  in the cavity, to which the change

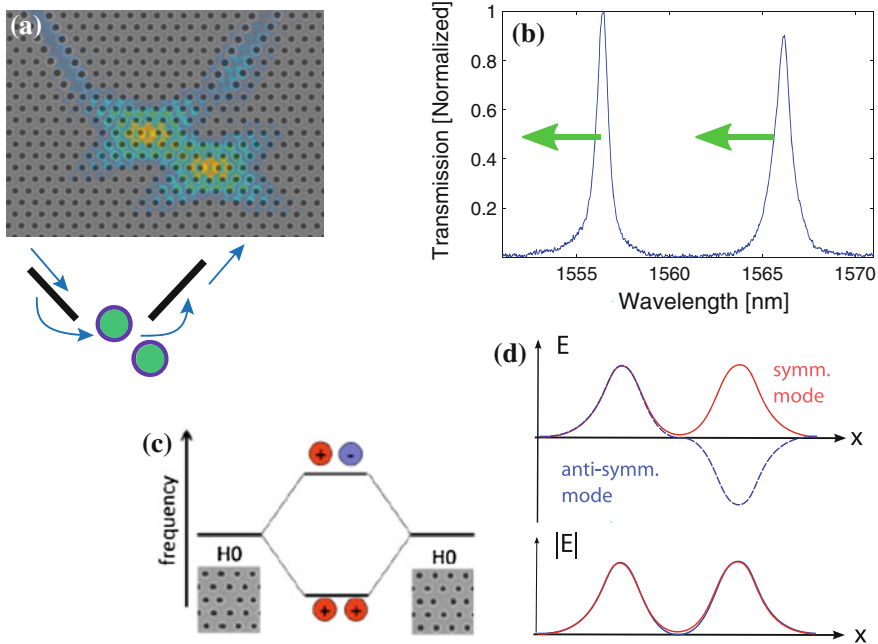


**Fig. 5.12** **a** SEM image of a Photon Molecule and, superimposed, the electric field energy density at resonance; **b** experimental transmission spectrum, arrows indicate the effect of the excitation of free-carriers; **c-d** concept of a Photon Molecule with associated odd and even modes

in the refractive index  $\Delta n$  is proportional, builds up depending on the simple rate equation  $\partial_t N_{\text{eff}} = -N_{\text{eff}}/\tau_{\text{carr}} + G(t)$ . Therefore, if the carrier lifetime  $\tau_{\text{carr}}$  is shorter than the duration of the excitation  $G(t)$ , carriers cannot accumulate, and the response is weak. Conversely, if the carrier lifetime is long, the recovery time of the all-optical device increases accordingly. Considering this, the optimized carrier lifetime should be ideally close to the duration of the excitation. This is illustrated in Fig. 5.13, where free carriers are excited into a nonlinear resonator by a pump pulse with duration  $t_{\text{pulse}} = 4.5$  ps, which is a sensible choice for processing data at a fast rate (e.g. time demultiplexing a 100 Gb/s data stream) and, therefore, suggests that carrier lifetime should be of the same order.

In the following, we will survey recent experiments where a variety of materials have been used to build a PhC all-optical gate. The recovery dynamics of a nonlinear photonic molecule is measured through a time resolved spectral transmission experiment (Fig. 5.14). The doublet of resonances allows to excite the cavity with a pump tuned to one resonance, while a spectrally broad pulse is used as a “white light” source to probe the instantaneous transmission spectrum of the other resonance. Both pump and probe are obtained from the same mode-locked laser (MLL) by spectral filtering.

The dynamical response of these nonlinear cavities is modelled by a combination of time-dependent coupled mode theory [42] and the dynamical equations



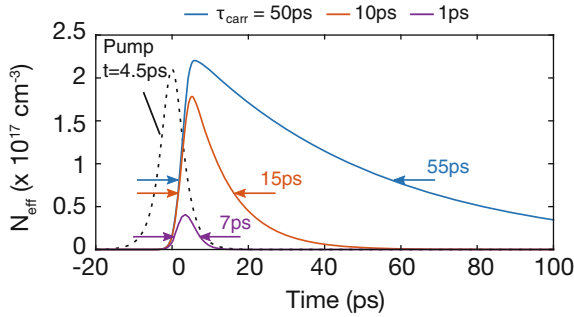


**Fig. 5.13** Calculated temporal decay of the effective carrier concentration, depending on different carrier lifetime:  $\tau_{\text{carr}} = 1, 10,$  and  $50 \text{ ps}$ . From [50]

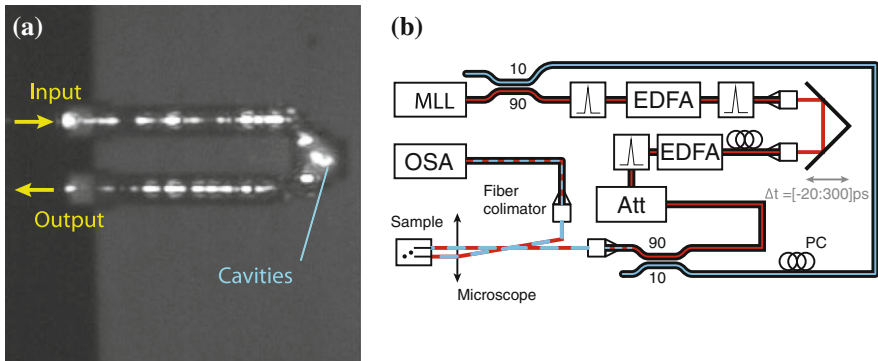


**Fig. 5.14** **a** Infra-red image (*top view*) of the PhC all-optical gate showing the access waveguides and the cavities from the top. On resonance, light propagates through the photon molecule and returns to the end-facet. **b** Spectrally and temporally resolved pump-probe experiment. Pump path (*red*), probe (*blue*). EDFA: Erbium Doped Fibre Amplifier, PC: Polarization Controller, Att: Attenuator, OSA: Optical Spectrum Analyser. Experimental setup from [49]

describing the evolution of the population of free carriers inside the resonator. Here, the diffusion of the photo-excited carriers is taken into account rigorously, within the ambipolar approximation, using the formalism of the Green's function. The model is able to reproduce the experimentally measured response accurately and with a minimal set of fitting parameters, namely the surface recombination velocity [48, 50].

### 5.4.3 InP

Nonlinear photonic crystal resonators, all based on the  $H_0$  design and made of InP, have been introduced recently [16, 29, 78, 86] and all the measurements of the

dynamical response have evidenced a fast and a slow time constant. A similar behaviour, but at a much lower pump excitation power, has also been reported in InGaAsP resonators [55]. The observed fast time constant, describing the decay of the transmitted probe, has been reported to be as low as 10 ps. Interestingly, this does not correspond to the relaxation of the carrier population, which is much longer. Rather, it results from the much faster diffusion process. Moreover, the transmission also depends on the detuning of the probe relative to the cavity, which can be optimized to obtain a short gating function. This is apparent in Fig. 5.15, showing the measured decay of the excited carriers, which is directly related to the instantaneous detuning of the resonator. Our model is in very good agreement with the experiment when assuming surface recombination velocity  $S = 10^3$  m/s which the only free parameter here (all the others are either calculated, or measured independently). Put in other words, the surface recombination can be deduced from pump-probe measurements [48].

It has been shown that the dynamical response can be further improved by modifying the lineshape and the symmetry of the resonator [85]. Still, the underlying dynamics is much slower than the observed response. This implies that free carriers will continue to accumulate if the repetition rate of the pulsed excitation is faster than the time required for a complete recovery of the carrier population.

#### 5.4.4 P-Doped InP

In an undoped, unbiased semiconductor, the decay of the effective density of the photo-excited carriers is governed by the ambipolar diffusion constant. In III–V materials such as GaAs, the process is dominated by the heavy holes. A much faster diffusion is achieved owing to p-doping, such that only the dynamics of the minority

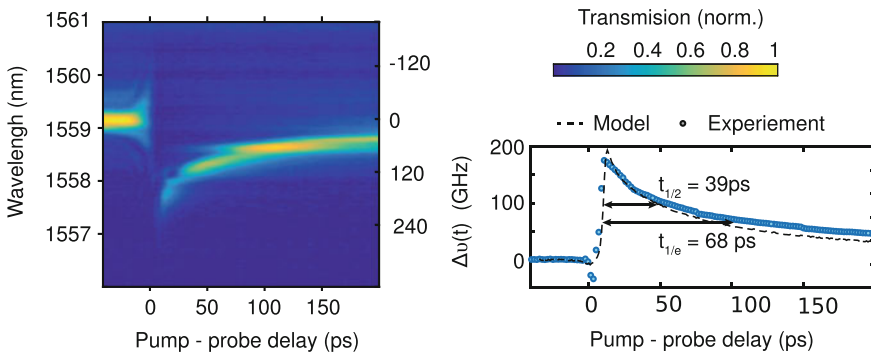


**Fig. 5.15** Pump-probe measurement of the InP gate described in [16]. *Left* spectrally and temporally resolved transmission map; *right* extracted instantaneous spectral shift (*circles*) and model (*dashed line*) with  $S = 10^3$  m/s

carriers, the highly mobile electrons, matters. This is a well known technique to accelerate the carrier dynamics and was, for instance, already used in uni-traveling carrier photodiodes [69].

This idea has been exploited to accelerate the response of an InP photonic molecule, which is doped with acceptors to the level of about  $10^{17} \text{ cm}^{-3}$ , such that free-carrier losses do not affect the Q factor ( $\alpha \simeq 1 \text{ cm}^{-1}$ ). The response is shown in Fig. 5.16, which clearly reveals a faster recovery, compared to the identical yet undoped structure in Fig. 5.15. More precisely, from the instantaneous spectral shift of the cavity it is deduced that the density of the excited carriers has halved within only  $\tau_{1/2} = 25 \text{ ps}$ , almost twice as fast as the undoped case.

As the optical excitation becomes stronger and the level of injected carriers becomes larger than the doping level, the ambipolar diffusion regime is eventually restored and the fast time constant increases again, as apparent in Fig. 5.17. A model

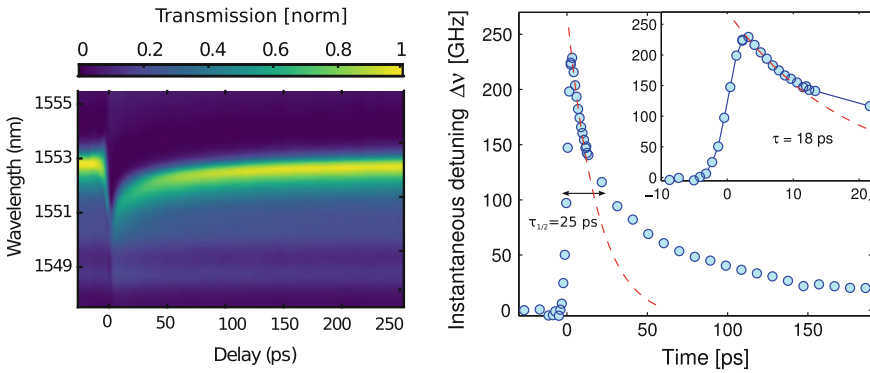


**Fig. 5.16** **a** Time-resolved experimental transmission spectra centred around the low-energy resonance **b** Extracted time-resolved instantaneous detuning. The double arrow indicates the time for halving the detuning  $\tau_{1/2}$ . The inset is an enlarged view with exponential fit (dashed line) and corresponding time constant  $\tau$ . From [49]

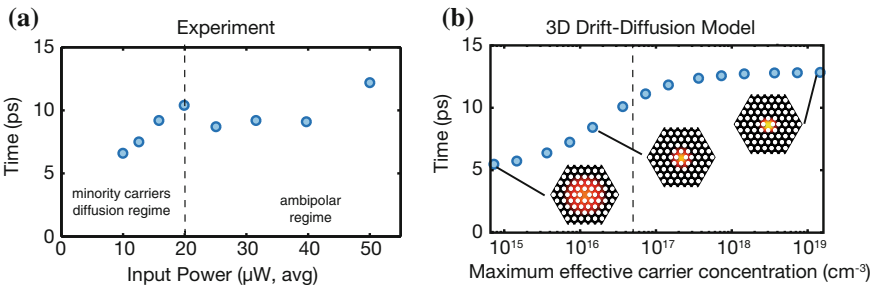


**Fig. 5.17** **a** Measured fast time constant as a function of the input pump power coupled to the cavities. **b** Calculated time constant versus the maximum of the effective carrier density. The dotted line represents the level of p-doping. The distribution of the electrons at  $t = 10 \text{ ps}$  is represented in the insets for different excitation levels. From [49]

accounting for the drift-diffusion process in the geometry of the PhC cavity reproduces this behaviour fairly well. P-doping is shown to be effective in enhancing the fast diffusion dynamics in PhC microresonators, without increasing the switching energy (still in the 100 fJ range) [49].

### 5.4.5 Passivated GaAs

As discussed in Sect. 5.4, the optical nonlinear response related to the excitation of free carriers is particularly fast in Gallium Arsenide, because the strong surface recombination induces a fast recovery by quickly removing carriers. However, it turns out that this effect is so strong in photonic crystal devices that it prevents the build-up of the free carrier population, thereby dwarfing nonlinear response. Another issue which has been observed in GaAs PhC is the degradation of the optical properties of the resonator, due to photo-induced oxidation [40].

The passivation of semiconductor surfaces exposed to large optical power densities, such as at the end facets of high-power laser diodes is well known and it is dealt with conventional deposition techniques such as PECVD (plasma-assisted chemical vapour deposition). These known passivation techniques have been used to improve the quality of the PhC surfaces. The trouble here is the complex geometry of PhC membranes, requiring a conformal coating of the surface, including that facing the semiconductor substrate, which is hardly accessible. Nevertheless, a new technique, known as Atomic Layer Deposition (ALD) has been developed, mainly in the context of high-speed electronics based on III–V semiconductors [6, 84] and has been applied to PhC very recently [38]. However, the impact on the surface recombination of ALD, depending on the specific treatment of the surface and the material deposited have been evidenced later [50]. Figure 5.18 shows a 30 nm thick layer of  $\text{Al}_2\text{O}_3$  covering all the surfaces of a GaAs PhC uniformly.

Spectrally and temporally resolved pump-probe experiments have been carried out to compare the relaxation dynamics before and after passivation with  $\text{Al}_2\text{O}_3$ . The main result is summarized in Fig. 5.19a, b, demonstrating that the specific surface passivation treatment used here results into an increase of the instantaneous detuning from about 30 GHz to 140 GHz. Furthermore, the non-instantaneous recovery of the detuning is now apparent, which is consistent with an increase of the carrier lifetime. Importantly, the two measurements (passivated and unpassivated) are both reproduced accurately by the model [48]. The change of a single parameter, the surface recombination velocity, accounts for the different response. We conclude that a fairly large value,  $S = 10^5 \text{ ms}^{-1}$ , about the saturation velocity in GaAs, is characteristic of the uncoated sample, while ALD reduces drastically the recombination to  $3 \times 10^3 \text{ ms}^{-1}$ , i.e. by nearly two orders of magnitude. The modelled decay of the carrier density in the cavity (Fig. 5.19c) is insightful and reveals the drastic change of dynamics induced by the ALD coating.

Spectrally non-degenerate homodyne pump-probe measurements are used to estimate the response of the switch. When the pump and the probe are set with optimal

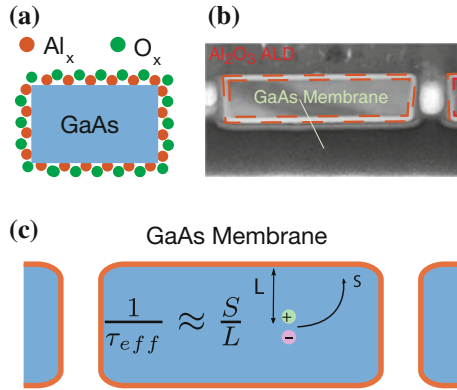


**Fig. 5.18** **a** Atomic Layer Deposition process **b** Cross-sectional transmission electron micrograph (TEM) of the PhC slab revealing a conformal  $\text{Al}_2\text{O}_3$  coating [50] and **c** schematics of the surface recombination process

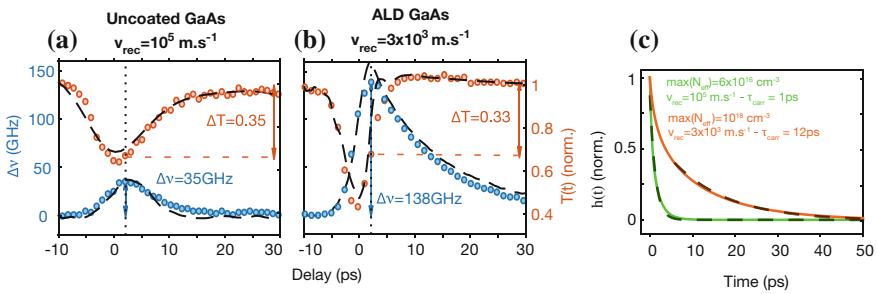


**Fig. 5.19** Instantaneous cavity frequency shift  $\Delta v(t) = v_c(t) - v_c(-\infty)$  (left scale) and time-resolved transmission  $T(t)$  (right scale), for respectively the uncoated **(a)** and coated **(b)** samples. Note that in the case of the uncoated GaAs **(a)** the response is almost instantaneous, only limited by the pulse duration (4 ps) and the cavity lifetime. In both cases, the coupled pump energy is estimated to 300 fJ. The calculated response is superimposed (solid dashed line) **c** Calculated normalized effective carrier density  $h(t)$  for both reference (green) and ALD (orange) samples in order to extracted the carrier lifetimes  $\tau$ . From [50]

detuning relative to the resonances (Fig. 5.20), a switching contrast of 7 dB is achieved with a maximum of 200 fJ per pulse. If the pulse energy is decreased to about 100 fJ, the contrast is still 3 dB, enough to perform some all-optical processing operations corresponding to a power consumption of 1 mW for 10 giga operations/s, which can be considered as energy-efficient. It is remarkable that the transmission has recovered completely in about 20 ps, the  $1/e$  decay being about 12 ps, which is extremely fast for a semiconductor device based on free carriers.

A stronger evidence of a fast and complete recovery is the capability to respond to a sequence of closely spaced pulses. In fact, this implies that any possible “internal” dynamics has relaxed. Figure 5.21 reports the excitation of the AOG with two pump pulses with spacing decreasing from 40 ps to 10 ps. The probe reveals that the

**Fig. 5.20** Time-resolved homodyne non-degenerate pump-probe measurements at probe detuning  $\Delta\lambda = -2.2$  nm. Relative probe transmission  $T/T(-\infty)$  versus pump-probe delay and extracted rise-time  $t_r$ , fall time  $t_f$  and width at  $1/e$ . From [50]

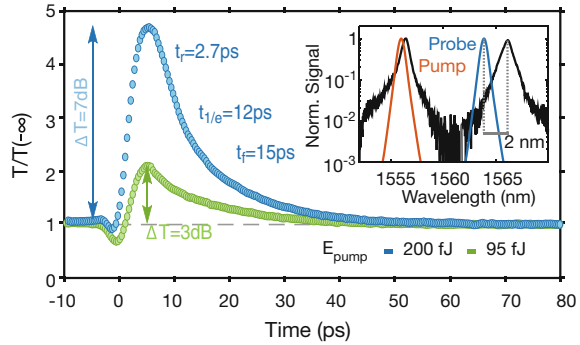
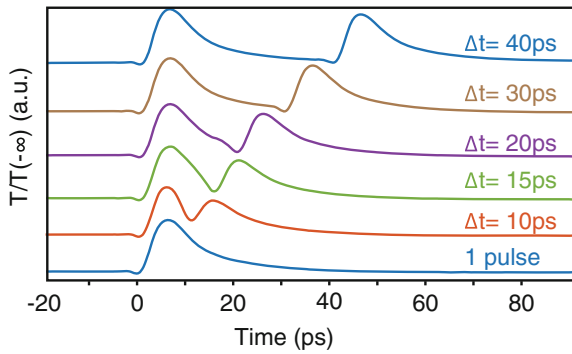


**Fig. 5.21** Same as Fig. 5.20 but with a sequence of two pump pulses with separation  $\Delta t$  varying from 10 ps to 40 ps. From [50]



response to the following pulse is identical, hence not influenced by any transient dynamics due to the first pulse, until these are very close.

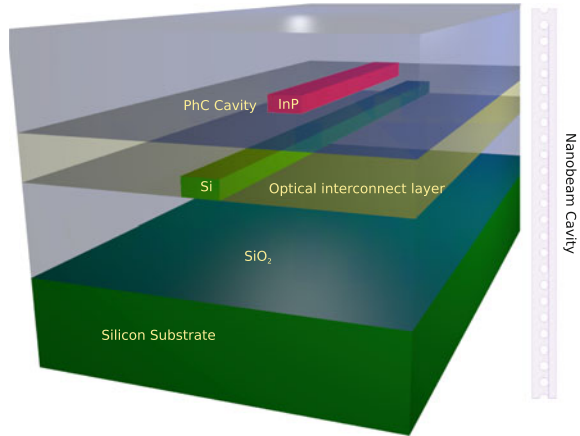
### 5.4.6 Integration with Silicon Photonics

In the context of all-optical switching based on the excitation of free carriers, compound III–V semiconductors can offer a larger electron mobility, hence a potentially faster response, than Silicon. Moreover, their direct electronic band gap can be adjusted by a suitable choice of the compound, which here is exploited to maximize the nonlinear response. Still, Silicon Photonics provides an industrial-grade platform for integrated optical circuits with a broad range of functionalities already available and the capacity of addressing complicated architectures.

The hybrid integration of III–V devices on a silicon photonic chip address this point as it allows to combine the advantages of the Silicon platform with the unique properties of III–V. The most mature and accessible approach to hybrid integration relies on the adhesive wafer bonding [28].

The integration of nanopatterned structures such as PhCs is however challenging because of the extremely accurate alignment required to control the coupling to the

**Fig. 5.22** Nanobeam cavity made of InP heterogeneously integrated on a Silicon Photonic Chip, [7]



underlying silicon waveguide (Fig. 5.22). Nonetheless, a “nanobeam” PhC resonator made of InP has been fabricated on top of a silicon photonic circuit [25]. The III–V structure is entirely encapsulated in Silica, which provides an additional advantage in terms of better thermal sinking, particularly important for laser sources [8].

By adding a InGaAsP thin layer at both surfaces of the InP membrane, surface recombination is greatly increased, which translates into a much faster recovery of the nonlinear response. By exploiting this property, a fast optical gate with a recovery time of about 30 ps has been demonstrated. Furthermore, all-optical wavelength conversion and signal recovery have been demonstrated at a rate as high as 10 Gb/s [7]. This landmark experiment demonstrates the feasibility of complex photonic circuits including sources, amplifiers and all-optical gates.

## 5.5 Application Example: All-Optical Signal Sampling

The “digital world” surrounding us is actually physically supported by analog signals, as well as any other signal associated to sounds, images, or any kind of physical measurement. The transition from the analog to the digital domain for processing, requires analog-to-digital converters (ADC). An A/D-converter produces a digital representation, a sample, of an analog signal. The two main characteristics of ADCs are the sampling rate and the accuracy of the sample expressed as the number of representative bits (ENOB). The need for fast ADCs with a large dynamic range (equivalently large ENOB) originates from some application domains such as medical imaging, broadband communications and radar [22]. Despite the steady progress of electronics, the current ADCs are struggling to meet the required performances.

While the thermal noise has been identified as the dominant limiting factor for high-resolution ADCs operating at moderate sampling rates (e.g. audio), the performances of high-speed ADCs are limited by both the comparator ambiguity and by

the timing error (jitter) in opening the gate. Concerning the latter issue, it has been shown that timing jitter in state-of-the-art electronic clocks is hardly better than 100 fs. This affects the accuracy of the representation, explaining why the ENOB has not increased much in fast ADCs [5]. For instance, Fujitsu has demonstrated a 65 GSa/s ADC providing 8-Bit resolution [1].

In contrast to electronic clocks, mode locked lasers (MLLs) can generate a train of optical pulses spaced by extremely regular time intervals, and therefore used as a high-quality optical clock. The lowest time jitter reported is below 1 fs [37], i.e. orders of magnitude better than electronic clocks. Not surprisingly, this has prompted a radically new approach to ADCs involving the use of an optical clock signal [5]. We note that if the signal to be sampled is also in the optical domain, an AOG is required.

In fact, the combination of a MLL and a electro-optic modulator is likely to be the simplest approach for converting an analog microwave signal into a train of samples. This architecture also allows a substantial degree of parallelisation owing to photonic integration [5]. If, however, the microwave signal is provided in the optical domain, which is the common situation of microwave photonics [60], then one might speculate about the possibility of performing sampling all-optically, by mixing the optical clock and the signal.

Another important performance factor in ADCs is the power consumption, in particular regarding high-speed applications in embarked devices, where the power dissipation and the operating time of the battery are critical. In fact, it has been shown that the power consumption of an electronic ADCs scales approximately quadratically with the sampling frequency (see Fig. 5.23), and therefore this becomes a concern when large bandwidth is needed. Moreover, power consumption also depends critically on the number of bits. For instance, ADCs with sampling frequency equal to 20 GHz consume 1.2 W with a 6 bit resolution and 10 W with 8 bits [57, 59]. Thus, the power consumption of an AOG operating at high-speed and with a large dynamics (switching contrast) is extremely important. A less critical of power consumption on the speed is therefore a crucial and achievable goal in optical signal processing.

### 5.5.1 All-Optical Sampling

An example of all-optical sampling involving a PhC AOG is shown here. A RF sinusoidal signal with frequency  $f_{MZ} = 2.777$  GHz is transposed in the optical domain using a Mach-Zehnder modulator (MZM) and then it is sampled by PhC AOG described in Sect. 5.4.1, made of Indium Phosphide. The device is activated by train of pulses generated by a Mode Locked Laser (MLL) serving as optical clock with frequency equal to  $f_{clock} = 2.525$  GHz. The wavelengths of the two optical inputs are adjusted such as the clock is set on the resonance at higher frequency whereas the optical carrier is blue detuned by about 1 nm from the low frequency resonance. The sampled signal is collected at the output, separated from the clock by spectral



**Fig. 5.23** Power consumption of an Analog to Digital Converter depending on the sampling rate (image adapted from [20])

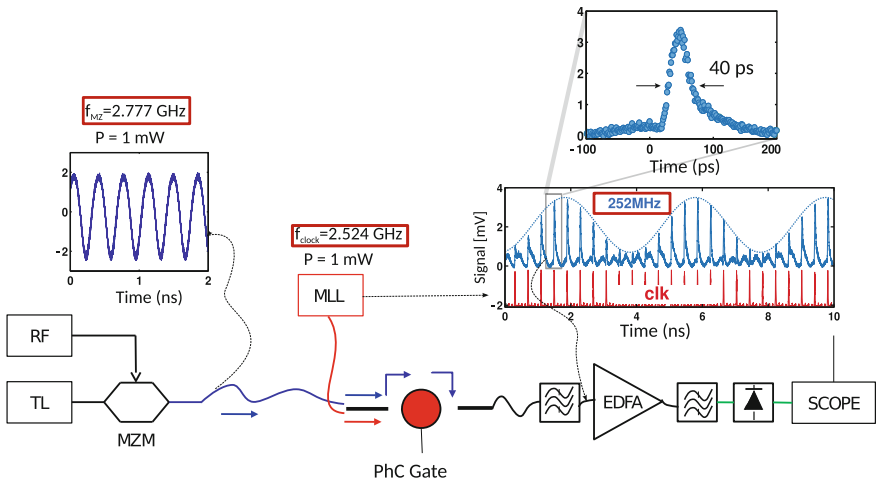
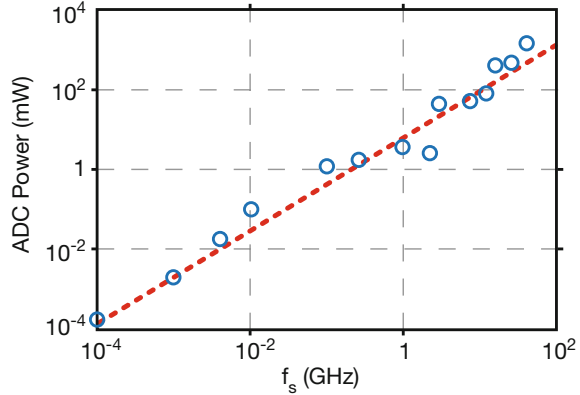


**Fig. 5.24** Experiment of all-optical sampling involving a PhC AOG. Inputs tunable laser (TL) modulated by a Mach-Zehnder Modulator (MZM) shown in the inset, and Mode Locked Laser (MLL). Output is filtered and amplified by an Erbium Doped Fiber Amplifier (EDFA), detected and imaged at the oscilloscope (insets)

filtering and amplified by an optical low-noise amplifier (EDFA) to raise the power level before the InGaAs photodetector. The sampled signal is then displayed together with the clock and the input signal by an oscilloscope synchronised with the MLL (Fig. 5.24).

In this experiment, the sampling frequency is smaller than the signal frequency, thus the sampled signal represents an aliased version of the original signal, which is a sinusoid with frequency  $f = f_{MZ} - n f_{clock} = 252 \text{ MHz}$ , as the original signal is located in the second Nyquist band ( $n = 1$ ). Considering a more general signal centred at some frequency  $f_0$  with spectral width smaller than  $f_{clock}/2$ , then the sampling generates a representation of the original signal in the base (low frequency)

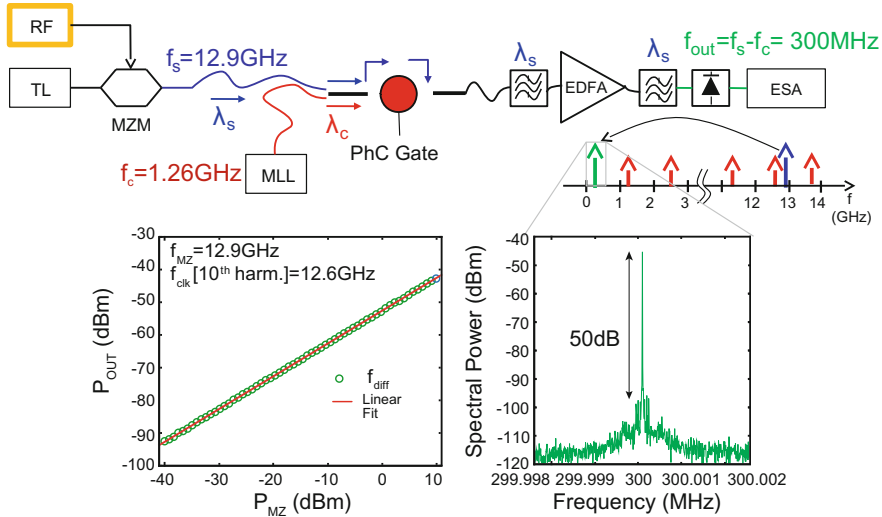


**Fig. 5.25** All-optical sampling involving a PhC AOG, observed in the electric spectral domain. Experimental set up (top), as in Fig. 5.24, with an electrical spectrum analyser (ESA) replacing the oscilloscope. The harmonics of the clock are associated to the Nyquist's bands. Signals with frequency larger than the sampling frequency are translated into the first Nyquist band. Electric spectral power of the sampled signal as a function of the driving RF power applied to the MZM (bottom left) and electric spectrum of the sampled signal (bottom right)

band which is “exact” in the sense of the Shannon criterion. This has an extremely important implication in the domain of wide band radio receivers and radars, as there sampling also implements the frequency down-conversion.

This is clearly seen in another measurement. Here, a RF signal at a much higher frequency (12.9 GHz) is sampled with a clock at 1.26 GHz. The all-optical sampling generates a replica in the first Nyquist band at 300 MHz, corresponding to the mixing with the 10th harmonic of the clock of the signal. The RF spectrum is a narrow lineshape with noise being 50 dB below (Fig. 5.25). Another interesting point is the relationship between the input and sampled signal amplitudes. This is remarkably linear when the input RF power is spanned over 50 dB.

This linear dependence is not obvious, given the nonlinear character of the AOG. Nonetheless, an intuitive explanation for this is in the mechanism involved in the sampling operation i.e. the two-photon absorption, as explained in Sect. 5.3. In spite the fact that the average power of the two incoming optical signals is similar (about 1 mW), the peak power of the clock is much larger than the signal that only the former triggers the nonlinear response trough the two-photon absorption.

The most attractive aspect of this approach to photonic ADC is that the implementation of a series to parallel scheme is conceptually easy. There, a high-speed signal is sampled by time-interleaved ADCs operating in parallel and feeding lower speed

electronic digitizers. Besides ADCs, AOGs can be used for wavelength conversion, pulse analysis [79], signal regeneration and optical time demultiplexing.

## 5.6 Conclusions

Historically, nonlinear optical effects have been evidenced using large optical power levels, which have been made possible by the invention of the laser. This is why energy-efficiency and nonlinear optics are regarded to be at odds. The main point of this chapter is to bring evidences that this is no longer true. New material processing techniques have enabled the creation of a variety of dielectric optical resonators capable of nearly diffraction-limited optical confinement. Consequently, electric fields large enough to trigger nonlinear effects are achieved in tiny volumes by exciting the resonator with optical power levels in the mW or even the  $\mu W$  range, namely many orders of magnitude weaker than in more common nonlinear optic experiments.

The kind of resonators considered here are made of III–V semiconductor compounds and the optical confinement is based on the Bragg scattering, and are named Photonic Crystals. The nonlinear mechanism exploited here is the excitation of free carriers due to the nonlinear absorption, which reach a large density in the resonator. This produces a change in the refractive index which can be exploited to detune the resonance dynamically and, hence, to create an all-optical gate.

Aiming both at a fast response and energy-efficiency implies a trade off, as, in general, faster effects are weaker, e.g. free-carrier versus thermo-optic index change. Nonetheless, extremely fast nonlinear devices which could be operated with mW of optical pump have been demonstrated, by exploiting the choice offered by compound III–V semiconductors, and the possibility to control the dynamics of free carriers through surface treatment, doping, and the geometry. Moreover, it has been shown that such devices can be integrated on a silicon photonic platform, and thereby offering radically novel functionalities which could be combined with the panoply already available there, to create advanced devices for optical signal processing.

**Acknowledgements** We acknowledge support from the French Research Agency (ANR) through the contracts Qswitch, Auctopuss and Ethan, and the European Commission, through the contracts Qphoton, Gospel, Copernicus. We thank Fabrice Raineri, Johann-Peter Reithmaier and Gadi Eisenstein for fruitful discussions.

## References

1. Fujitsu europe press release, fujitsu launches second generation ultra-fast 65 GSa/s 8-bit ADC technology for 100G optical transport (2010), [http://www.fujitsu.com/emea/news/pr/fseu-en\\_20100913-978.html](http://www.fujitsu.com/emea/news/pr/fseu-en_20100913-978.html)
2. Y. Akahane, T. Asano, B.S. Song, S. Noda, High-Q photonic nanocavity in a two-dimensional photonic crystal. *Nature* **425**(6961), 944–947 (2003)

3. R. Akimoto, S. Gozu, T. Mozume, H. Ishikawa, Monolithically integrated all-optical gate switch using intersubband transition in InGaAs/AlAsSb coupled double quantum wells. *Opt. Exp.* **19**(14), 13386–13394 (2011)
4. V.R. Almeida, M. Lipson, Optical bistability on a silicon chip. *Opt. Lett.* **29**(20), 2387–2389 (2004)
5. M.E. Grein, A.H. Nejadmalayeri, C.W. Holzwarth, M.Y. Sander, M.S. Dahlem, Y. Michael, P. Michael, W. Geis Nicole, A. DiLello Jung, U. Yoon Ali Motamedi... E.P. Ippen, A. Khilo, S.J. Spector, F.X. Krtner, Photonic ADC: Overcoming the bottleneck of electronic jitter. *Optics Express* **20**(4), 4454 (2012)
6. T. Aoki, N. Fukuhara, T. Osada, H. Sazawa, M. Hata, T. Inoue, Nitride passivation reduces interfacial traps in atomic-layer-deposited Al<sub>2</sub>O<sub>3</sub>/GaAs (001) metal-oxide-semiconductor capacitors using atmospheric metal-organic chemical vapor deposition. *Appl. Phys. Lett.* **105**(3), 033513 (2014)
7. A. Bazin, K. Lenglé, M. Gay, P. Monnier, L. Bramerie, R. Braive, G. Beaudoin, I. Sagnes, R. Raj, F. Raineri, Ultrafast all-optical switching and error-free 10 Gbit/s wavelength conversion in hybrid InP-silicon on insulator nanocavities using surface quantum wells. *Appl. Phys. Lett.* **104**(1), 011102 (2014)
8. A. Bazin, P. Monnier, X. Lafosse, G. Beaudoin, R. Braive, I. Sagnes, R. Raj, F. Raineri, Thermal management in hybrid InP/silicon photonic crystal nanobeam laser. *Opt. Express* **22**(9), 10570–10578 (2014)
9. B.R. Bennett, R.A. Soref, J.A. del Alamo, Carrier-induced change in refractive index of InP, GaAs and InGaAsP. *Quantum Electron. IEEE J.* **26**(1), 113–122 (1990)
10. R. Bose, J.S. Pelc, S. Vo, C.M. Santori, R.G. Beausoleil, Carrier dynamics in GaAs photonic crystal cavities near the material band edge. *Opt. Express* **23**(10), 12732 (2015)
11. A.D. Bristow, J.-P.R. Wells, W.H. Fan, A.M. Fox, M.S. Skolnick, D.M. Whittaker, A. Tahraoui, T.F. Krauss, J.S. Roberts, Ultrafast nonlinear response of AlGaAs two-dimensional photonic crystal waveguides. *Appl. Phys. Lett.* **83**(5), 851 (2003)
12. J. Capmany, D. Novak, Microwave photonics combines two worlds. *Nat. Photonics* **1**(6), 319–330 (2007)
13. N. Cazier, X. Checoury, L.-D. Haret, P. Boucaud, High-frequency self-induced oscillations in a silicon nanocavity. *Opt. Express* **21**(11), 13626–13638 (2013)
14. S. Combré, S. Bansropun, M. Lecomte, O. Parillaud, S. Cassette, H. Benisty, J. Nagle, Optimization of an inductively coupled plasma etching process of Ga In P/Ga As based material for photonic band gap applications a. *J. Vac. Sci. Technol. B* **23**(4), 1521–1526 (2005)
15. Sylvain Combré, D. Rossi, Q.V. Tran, H. Benisty, GaAs photonic crystal cavity with ultrahigh Q: microwatt nonlinearity at 1.55  $\mu\text{m}$ . *Opt. Lett.* **33**, 1908–1910 (2008)
16. S. Combré, G. Lehoucq, A. Junay, S. Malaguti, G. Bellanca, S. Trillo, L. Menager, J.P. Reithmaier, A. De Rossi, All-optical signal processing at 10 GHz using a photonic crystal molecule. *Appl. Phys. Lett.* **103**(19), 193510 (2013)
17. G.W. Cong, R. Akimoto, K. Akita, T. Hasama, H. Ishikawa, Low-saturation-energy-driven ultrafast all-optical switching operation in (CdS/ZnSe)/BeTe intersubband transition. *Opt. Express* **15**(19), 12123–12130 (2007)
18. N.J. Doran, D. Wood, Nonlinear-optical loop mirror. *Opt. Letters* **13**(1), 56–58 (1988)
19. H.J.S. Dorren, M.T. Hill, Y. Liu, N. Calabretta, A. Srivatsa, F.M. Huijskens, H. de Waardt, G.D. Khoe, Optical packet switching and buffering by using all-optical signal processing methods. *J. Lightwave Technol.* **21**(1), 2–12 (2003)
20. M. Elbadry, R. Harjani, *Quadrature Frequency Generation for Wideband Wireless Applications*. Springer (2015)
21. M.A. Foster, A.C. Turner, J.E. Sharping, B.S. Schmidt, M. Lipson, A.L. Gaeta, Broad-band optical parametric gain on a silicon photonic chip. *Nature* **441**(7096), 960–963 (2006)
22. P. Ghelfi, F. Laghezza, F. Scotti, G. Serafino, A. Capria, S. Pinna, D. Onori, C. Porzi, M. Scaffardi, A. Malacarne, V. Vercesi, E. Lazzeri, F. Berizzi, A. Bogoni, A fully photonics-based coherent radar system. *Nature* **507**(7492), 341–345 (2014)

23. H.M. Gibbs, S.L. McCall, T.N.C. Venkatesan, A.C. Gossard, A. Passner, W. Wiegmann, Optical bistability in semiconductors. *Appl. Phys. Lett.* **35**(6), 451 (1979)
24. H.M. Gibbs, S.L. McCall, T.N.C. Venkatesan, Differential gain and bistability using a sodium-filled fabry-perot interferometer. *Phys. Rev. Lett.* **36**(19), 1135–1138 (1976)
25. Y. Halioua, A. Bazin, P. Monnier, T.J. Karle, G. Roelkens, I. Sagnes, R. Raj, F. Raineri, Hybrid III-V semiconductor/silicon nanolaser. *Opt. Express* **19**(10), 9221–9231 (2011)
26. K.L. Hall, J. Mark, E.P. Ippen, G. Eisenstein, Femtosecond gain dynamics in InGaAsP optical amplifiers. *Appl. Phys. Lett.* **56**(18), 1740 (1990)
27. T.D. Happ, M. Kamp, A. Forchel, J.-L. Gentner, L. Goldstein, Two-dimensional photonic crystal coupled-defect laser diode. *Appl. Phys. Lett.* **82**(1), 4–6 (2003)
28. M.J.R. Heck, H.-W. Chen, A.W. Fang, B.R. Koch, D. Liang, H. Park, M.N. Sysak, J.E. Bowers, Hybrid silicon photonics for optical interconnects. *IEEE J. Sel. Topics Quantum Electron.* **17**(2), 333–346 (2011)
29. M. Heuck, S. Combr e, G. Lehoucq, S. Malaguti, G. Bellanca, S. Trillo, P.T. Kristensen, J. M ork, J.P. Reithmaier, A. de Rossi, Heterodyne pump probe measurements of nonlinear dynamics in an indium phosphide photonic crystal cavity. *Appl. Phys. Lett.* **103**(18), 181120 (2013)
30. C. Husko, A. De Rossi, S. Combr e, Q. V Tran, F. Raineri, C.W. Wong, Ultrafast all-optical modulation in GaAs photonic crystal cavities. *Appl. Phys. Lett.* **94**(2), 021111 (2009)
31. S. Ishii, K. Nozaki, T. Baba, Photonic molecules in photonic crystals. *Jap. J. Appl. Phys.* **45**(8A), 6108–6111 (2006)
32. P. Bermel, S.G. Johnson, J.D. Joannopoulos, J. Bravo-Abad, A. Rodriguez, M. Solja ic, Enhanced nonlinear optics in photonic-crystal microcavities. *Opt. Express* **15**(24) (2007)
33. J.L. Jewell, S.L. McCall, A. Scherer, H.H. Houh, N.A. Whitaker, A.C. Gossard, J.H. English, Transverse modes, waveguide dispersion, and 30 ps recovery in submicron GaAs/AlAs microresonators. *Appl. Phys. Lett.* **55**(1), 22 (1989)
34. S. John, Strong localization of photons in certain disordered dielectric superlattices. *Phys. Rev. Lett.* **58**(23), 2486–2489 (1987)
35. S.G. Johnson, P.R. Villeneuve, S. Fan, J.D. Joannopoulos, Linear waveguides in photonic-crystal slabs. *Phys. Rev. B* **62**(12), 8212 (2000)
36. J.B. Khurgin, How to deal with the loss in plasmonics and metamaterials. *Nat. Nanotechnol.* **10**(1), 2–6 (2015)
37. T.K. Kim, Y. Song, K. Jung, C. Kim, H. Kim, C.H. Nam, J. Kim, Sub-100-as timing jitter optical pulse trains from mode-locked er-fiber lasers. *Opt. Lett.* **36**(22), 4443 (2011)
38. S. Kiravittaya, H.S. Lee, L. Balet, L.H. Li, M. Francardi, A. Gerardino, A. Fiore, A. Rastelli, O.G. Schmidt, Tuning optical modes in slab photonic crystal by atomic layer deposition and laser-assisted oxidation. *J. Appl. Phys.* **109**(5), 053115–053115 (2011)
39. T.F. Krauss, R.M. De La Rue, S. Brand, Two-dimensional photonic-bandgap structures operating at near-infrared wavelengths. *Nature* **383**(6602), 699–702 (1996)
40. H.S. Lee, S. Kiravittaya, S. Kumar, J.D. Plumhof, L. Balet, L.H. Li, M. Francardi, A. Gerardino, A. Fiore, A. Rastelli, O.G. Schmidt, Local tuning of photonic crystal nanocavity modes by laser-assisted oxidation. *Appl. Phys. Lett.* **95**(19), 191109 (2009)
41. S. Malaguti, G. Bellanca, A. De Rossi, S. Combr e, S. Trillo, Self-pulsing driven by two-photon absorption in semiconductor nanocavities. *Phys. Rev. A* **83**, 051802 (2011)
42. C. Manolatou, M.J. Khan, S. Fan, P.R. Villeneuve, H.A. Haus, J.D. Joannopoulos, Coupling of modes analysis of resonant channel add-drop filters. *IEEE J. Quantum Electron.* **35**(9), 1322–1331 (1999)
43. J. Mark, J. Mork, Subpicosecond gain dynamics in InGaAsP optical amplifiers: Experiment and theory. *Appl. Phys. Lett.* **61**(19), 2281 (1992)
44. D. Marpaung, C. Roeloffzen, R. Heideman, A. Leinse, S. Sales, J. Capmany, Integrated microwave photonics: Integrated microwave photonics. *Laser Photon. Rev.* **7**(4), 506–538 (2013)
45. A. Mart nez, J. Blasco, P. Sanchis, V. Jos e Gal n, J. Garc a-Rup rez et al., Ultrafast all-optical switching in a silicon-nanocrystal-based silicon slot waveguide at telecom wavelengths. *Nanoletters* **10**, 15061511 (2010)

46. M. Matsuura, O. Raz, F. Gomez-Agis, N. Calabretta, H.J.S. Dorren, 320 Gbit/s wavelength conversion using four-wave mixing in quantum-dot semiconductor optical amplifiers. *Opt. Lett.* **36**(15), 2910 (2011)
47. C. Meuer, C. Schmidt-Langhorst, R. Bonk, H. Schmeckebeier, D. Arsenijevic, G. Fiol, A. Galperin, J. Leuthold, C. Schubert, D. Bimberg, 80 Gb/s wavelength conversion using a quantum-dot semiconductor optical amplifier and optical filtering. *Opt. Express* **19**(6), 5134–5142 (2011)
48. G. Moille, S. Combrié, A. De Rossi, Modeling of the carrier dynamics in nonlinear semiconductor nanoscale resonators. *Phys. Rev. A* **94**, 023814 (2016)
49. G. Moille, S. Combrié, K. Fuchs, M. Yacob, J.P. Reithmaier, A. de Rossi, Acceleration of the nonlinear dynamics in p-doped indium phosphide nanoscale resonators. *Opt. Lett.* **42**, 795–798 (2017)
50. G. Moille, S. Combrié, L. Morgenroth, G. Lehoucq, F. Neuilly, H. Bowen, D. Decoster, A. de Rossi, Integrated all-optical switch with 10ps time resolution enabled by ald. *Laser Photon. Rev.* **10**(3), 409–419 (2016)
51. H.C.H. Mulvad, M. Galili, L.K. Oxenlwe, H. Hao, A.T. Clausen, J.B. Jensen, C. Peucheret, P. Jeppesen, Demonstration of 5.1 Tbit/s data capacity on a single-wavelength channel. *Opt. Express* **18**(2), 1438–1443 (2010)
52. M.P. Nezhad, A. Simic, O. Bondarenko, B. Slutsky, A. Mizrahi, L. Feng, V. Lomakin, Y. Fainman, Room-temperature subwavelength metallo-dielectric lasers. *Nat. Photon.* **4**(6), 395–399 (2010)
53. D.D. Nolte, Surface recombination, free-carrier saturation, and dangling bonds in InP and GaAs. *Solid-state Electron.* **33**(2), 295–298 (1990)
54. M. Notomi, S. Mitsugi, Wavelength conversion via dynamic refractive index tuning of a cavity. *Phys. Rev. A* **73**, 051803(R) (2006)
55. K. Nozaki, T. Tanabe, A. Shinya, S. Matsuo, T. Sato, H. Taniyama, M. Notomi, Sub-femtojoule all-optical switching using a photonic-crystal nanocavity. *Nat. Photon.* **4**(7), 477–483 (2010)
56. O. Painter, R.K. Lee, A. Scherer, A. Yariv, J.D. O'Brien, P.D. Dapkus, I. Kim, Two-dimensional photonic band-gap defect mode laser. *Science* **284**(5421), 1819–1821 (1999)
57. K. Poulton, R. Neff, B. Setterberg, B. Wuppermann, A 20-GSample/s 8b ADC with a 1-MByte Memory in 0.18- $\mu$ m CMOS. *IEEE International Solid State Circuits Conference Digest of Technical Papers* (2003)
58. D.F.Q. Xu, R.G. Beausoleil, Silicon microring resonators with 1.5- $\mu$ m radius. *Opt. Express* **16**(6), 4309 (2008)
59. P. Schvan, J. Bach, C. Falt, P. Flemke, R. Gibbins, Y. Greshishchev, N. Ben-Hamida, D. Pollex, J. Sitch, S.-C. Wang, J. Wolczanski, A 24GS/s 6b ADC in 90 nm CMOS. In *2008 IEEE International Solid-State Circuits Conference—Digest of Technical Papers*, pp. 544–634. IEEE (2008)
60. A.J. Seeds, Microwave photonics. *Microw. Theor. Tech. IEEE Trans.* **50**(3), 877–887 (2002)
61. H. Sekoguchi, Y. Takahashi, T. Asano, S. Noda, Photonic crystal nanocavity with a q-factor of 9 million. *Opt. Express* **22**(1), 916–924 (2014)
62. M. Sheik-Bahae, D.J. Hagan, E.W. Van Stryland, Dispersion and band-gap scaling of the electronic kerr effect in solids associated with two-photon absorption. *Phys. Rev. Lett.* **65**, 96–99 (1990)
63. M. Sheik-Bahae, D.C. Hutchings, D.J. Hagan, E.W. Van Stryland, Dispersion of bound electron nonlinear refraction in solids. *IEEE J. Quantum Electron.* **27**(6), 1296–1309 (1991)
64. W. Shockley, *Electrons and holes in semiconductors: with applications to transistor electronics*. Van Nostrand (1950)
65. G.A. Siviloglou, S. Suntsov, R. El-Ganainy, R. Iwanow, G.I. Stegeman, D.N. Christodoulides, R. Morandotti, D. Modotto, A. Locatelli, C. De Angelis, Enhanced third-order nonlinear effects in optical AlGaAs nanowires. *Opt. Express* **14**(20), 9377–9384 (2006)
66. M. Soljačić, J.D. Joannopoulos, Enhancement of nonlinear effects using photonic crystals. *Nat. Mater.* **3**, 211–219 (2004)
67. M. Soljačić, M. Ibanescu, S.G. Johnson, Y. Fink, J.D. Joannopoulos, Optimal bistable switching in nonlinear photonic crystals. *Phys. Rev. E* **66**(5) (2002)

68. G.I. Stegeman, E.M. Wright, N. Finlayson, R. Zanoni, C.T. Seaton, Third order nonlinear integrated optics. *Lightwave Technol. J.* **6**(6), 953–970 (1988)
69. N. Shimizu, T. Ishibashi, S. Kodama, T. Furuta, High-speed response of uni-traveling-carrier photodiodes
70. T. Tanabe, K. Nishiguchi, A. Shinya, E. Kuramochi, H. Inokawa, M. Notomi, K. Yamada, T. Tsuchizawa, T. Watanabe, H. Fukuda, H. Shinojima, S. Itabashi, Fast all-optical switching using ion-implanted silicon photonic crystal nanocavities. *Appl. Phys. Lett.* **90**(3), 031115–031115 (2007)
71. T. Tanabe, M. Notomi, S. Mitsugi, A. Shinya, E. Kuramochi, All-optical switches on a silicon chip realized using photonic crystal nanocavities. *Appl. Phys. Lett.* **87**(15), 151112 (2005)
72. T. Tanabe, H. Taniyama, M. Notomi, Carrier diffusion and recombination in photonic crystal nanocavity optical switches. *J. Lightwave Technol.* **26**(11), 1396–1403 (2008)
73. G. Tayeb, D. Maystre, Rigorous theoretical study of finite-size two-dimensional photonic crystals doped by microcavities. *J. Opt. Soc. Am. A* **14**(12), 3323–3332 (1997)
74. Q. Vy Tran, S. Combrié, P. Colman, A. De Rossi, Photonic crystal membrane waveguides with low insertion losses. *Appl. Phys. Lett.* **95**(6), 231104–231104 (2009)
75. K.J. Vahala, Optical microcavities. *Nature* **424**, 839–846 (2003)
76. G.C. Valley, Photonic analog-to-digital converters. *Opt. Express* **15**(5), 1955–1982 (2007)
77. V. Van, T.A. Ibrahim, P.P. Absil, F.G. Johnson, R. Grover, P.-T. Ho, Optical signal processing using nonlinear semiconductor microring resonators. *Sel. Topics Quantum Electron. IEEE J.* **8**(3), 705–713 (2002)
78. D. Vukovic, Y. Yu, M. Heuck, S. Ek, N. Kuznetsova, P. Colman, E. Palushani, J. Xu, K. Yvind, L. Oxenloewe et al., Wavelength conversion of a 9.35 Gb/s RZOOK signal in an Inp photonic crystal nanocavity. *Photon. Technol. Lett.* **26**(257) (2014)
79. I.A. Walmsley, C. Dorrer, Characterization of ultrashort electromagnetic pulses. *Adv. Opt. Photon.* **1**(2), 308 (2009)
80. E. Weidner, S. Combrié, A. De Rossi, N.V. Quynh, S. Cassette, Nonlinear and bistable behavior of an ultrahigh-Q GaAs photonic crystal nanocavity. *Appl. Phys. Lett.* **90**(1), 101118 (2007)
81. A.E. Willner, S. Khaleghi, M.R. Chitgarha, O.F. Yilmaz, All-optical signal processing. *J. Lightwave Technol.* **32**(4), 660–680 (2014)
82. E. Yablonovitch, Inhibited spontaneous emission in solid-state physics and electronics. *Phys. Rev. Lett.* **58**(20), 2059–2062 (1987)
83. A.M. Yacomotti, F. Raineri, C. Cojocar, P. Monnier, A. Levenson, R. Raj, Nonadiabatic dynamics of the electromagnetic field and charge carriers in high-Q photonic crystal resonators. *Phys. Rev. Lett.* **96**, 093901 (2006)
84. P.D. Ye, G.D. Wilk, M.M. Frank, Processing and characterization of III–V compound semiconductor MOSFETs using atomic layer deposited gate dielectrics. In Athanasios Dimoulas, Evgeni Gusev, PaulC. McIntyre, and Marc Heyns, editors, *Advanced Gate Stacks for High-Mobility Semiconductors*, vol. 27 of *Advanced Microelectronics*, pp. 341–361. Springer, Berlin Heidelberg (2007)
85. Y. Yi, Y. Chen, H. Hao, W. Xue, K. Yvind, J. Mork, Nonreciprocal transmission in a nonlinear photonic-crystal Fano structure with broken symmetry: Nonreciprocal transmission in a nonlinear Fano structure. *Laser Photon. Rev.* **9**(2), 241–247 (2015)
86. Y. Yi, M. Heuck, S. Ek, N. Kuznetsova, K. Yvind, J. Mørk, Experimental demonstration of a four-port photonic crystal cross-waveguide structure. *Appl. Phys. Lett.* **101**(25), 251113–251113 (2012)
87. Y. Yi, E. Palushani, M. Heuck, N. Kuznetsova, P.T. Kristensen, S. Ek, D. Vukovic, C. Peucheret, L.K. Oxenløwe, S. Combrié et al., Switching characteristics of an Inp photonic crystal nanocavity: Experiment and theory. *Opt. Express* **21**(25), 31047–31061 (2013)
88. Z. Zhang, M. Qiu, Small-volume waveguide-section high Q microcavities in 2D photonic crystal slabs. *Opt. Express* **12**(17), 3988–3995 (2004)